Received: 1 February 2024 | Revised: 31 July 2024 | Accepted: 1 August 2024

DOI: 10.1111/gcb.17473

Global Change Biology WILEY

RESEARCH ARTICLE

New tree height allometries derived from terrestrial laser scanning reveal substantial discrepancies with forest inventory methods in tropical rainforests

Louise Terryn[1] | Kim Calders[1] | Félicien Meunier[1] | Marijn Bauters[1,2] | Pascal Boeckx[2] | Benjamin Brede[3] | Andrew Burt[4] | Jerome Chave[5] | Antonio Carlos Lola da Costa[6,7] | Barbara D'hont[1] | Mathias Disney[8,9] | Tommaso Jucker[10] | Alvaro Lau[11] | Susan G. W. Laurance[12] | Eduardo Eiji Maeda[13,14] | Patrick Meir[15] | Sruthi M. Krishna Moorthy[1,16] | Matheus Henrique Nunes[14,17] | Alexander Shenkin[18] | Thomas Sibret[1,2] | Tom E. Verhelst[1] | Phil Wilkes[19,20] | Hans Verbeeck[1]

Correspondence
Louise Terryn, Q-ForestLab, Department of Environment, Ghent, Belgium.
Email: louise.terryn@ugent.be; terrynlouise@outlook.com

Funding information
UK NERC Independent Research Fellowship, Grant/Award Number: grant: NE/S01537X/1; BELSPO (Belgian Science Policy Office), Grant/Award Number: STEREO III programme - project 3D-FOREST (SR/02/35; Fonds Wetenschappelijk Onderzoek, Grant/Award Number: 1214723N; Investissement d'Avenir grants of the ANR, France, Grant/Award Number: CEBA: ANR-10-LABX-0025; ESA-ESRIN, Grant/Award Number: Forestscan (contract AO/1-9584/18/NL/AI) and QA4EO (contract AO/1-9629/19/I-NS); Bijzonder Onderzoeksfonds UGent

Abstract

Tree allometric models, essential for monitoring and predicting terrestrial carbon stocks, are traditionally built on global databases with forest inventory measurements of stem diameter (D) and tree height (H). However, these databases often combine H measurements obtained through various measurement methods, each with distinct error patterns, affecting the resulting H:D allometries. In recent decades, terrestrial laser scanning (TLS) has emerged as a widely accepted method for accurate, non-destructive tree structural measurements. This study used TLS data to evaluate the prediction accuracy of forest inventory-based H:D allometries and to develop more accurate pantropical allometries. We considered 19 tropical rainforest plots across four continents. Eleven plots had forest inventory and RIEGL VZ-400(i) TLS-based D and H data, allowing accuracy assessment of local forest inventory-based H:D allometries. Additionally, TLS-based data from 1951 trees from all 19 plots were used to create new pantropical H:D allometries for tropical rainforests. Our findings reveal that in most plots, forest inventory-based H:D allometries underestimated H compared with TLS-based allometries. For 30-metre-tall trees, these underestimations varied from −1.6 m (−5.3%) to −7.5 m (−25.4%). In the Malaysian plot with trees reaching up to 77 m in height, the underestimation was as much as −31.7 m (−41.3%). We propose a TLS-based pantropical H:D allometry, incorporating maximum climatological water deficit for site effects, with a mean uncertainty of 19.1% and a mean bias of −4.8%. While the mean uncertainty is roughly 2.3% greater than that of the Chave2014 model, this

For affiliations refer to page 15.

model demonstrates more consistent uncertainties across tree size and delivers less biased estimates of H (with a reduction of 8.23%). In summary, recognizing the errors in H measurements from forest inventory methods is vital, as they can propagate into the allometries they inform. This study underscores the potential of TLS for accurate H and D measurements in tropical rainforests, essential for refining tree allometries.

KEYWORDS
accuracy, forest inventory, terrestrial laser scanning, tree allometry, tree height, tropical rainforest

1 | INTRODUCTION

Tropical forests are home to some of the highest aboveground vegetation carbon stocks globally (Santoro et al., 2020). However, climate change and the ongoing processes of deforestation and forest degradation are causing these ecosystems to transition from carbon sinks to carbon sources, as evidenced by recent studies (Gatti et al., 2021; Hubau et al., 2020; IPCC, 2022). The impact of our warming climate is further exacerbating this situation, leading to increased tropical tree mortality rates and forest degradation at a global scale (Bauman et al., 2022; Lapola et al., 2023). Notably, large trees, which play a crucial role in sequestering carbon, are also highly susceptible to climate-induced stress, making them more vulnerable to drought-induced mortality (Bennett et al., 2015; Tavares et al., 2023). Consequently, there is a growing urgency to better understand the intricate relationship between tropical forests, their aboveground biomass (AGB) and the effects of climate warming. This understanding is crucial for predicting, monitoring and mitigating the consequences of climate change, as well as for devising improved management strategies for tropical forests.

AGB cannot be directly, non-destructively measured on site and is therefore, often estimated using allometric size-to-mass models from more easily measurable properties of stem diameter (D) and tree height (H) (Brown, 1997). When D, H and wood-specific gravity (or wood density) are known, a single AGB model can be applied across different tropical vegetation types with no detectable effect of the region or environmental factors (Chave et al., 2014). However, this is strongly contingent on the assumption of accurate H measurements or estimations. Several studies have stressed the significance of incorporating H into biomass estimations for tropical forests (Chave et al., 2014; Feldpausch et al., 2012). Tree height data are also instrumental in scaling AGB from local plots to regional and global levels using remote sensing techniques, underscoring the necessity for an extensive dataset of H for calibration and validation (Jucker et al., 2017). However, the available destructive calibration data for constructing these allometric models often suffer from limitations and biases, predominantly favouring smaller, more easily measured trees while underrepresenting larger ones (Burt et al., 2020; Calders et al., 2022). Consequently, this introduces uncertainties and biases into plot-scale allometric models, which in turn can propagate into regional and global models (Avitabile et al., 2016).

In tropical rainforests with dense canopies, accurately measuring H using forest inventory methods (e.g. measuring tape and poles for small trees, different hypsometers, ultrasonic and laser rangefinders, mechanical clinometers, physically climbing the tree with a tape measure, expert estimation and destructive methods), hereafter referred to as inventory methods, can be challenging, and data on H is often limited in quantity or accuracy (Hunter et al., 2013; Larjavaara & Muller-Landau, 2013). In such cases, individual H is estimated through the use of tree height-to-stem diameter (H:D) allometric relationships, which typically assume a constant H:D ratio, stem taper and crown-mass fraction (Feldpausch et al., 2011). Local H:D models offer more precise height estimations (Fayolle et al., 2016; Imani et al., 2017; Kearsley et al., 2013) because they inherently account for environmental conditions, forest structure and the disturbance history of the specific plot. Furthermore, Sullivan et al. (2018) demonstrated that by using a sample of just 50 trees per site (plot sizes ranging between 0.25 and 4.4 ha), including the 10 largest trees, one can develop local H:D models with low prediction errors. This approach significantly reduces sampling efforts, particularly for the largest trees, for which H measurement is often highly challenging or even unfeasible (Hunter et al., 2013; Larjavaara & Muller-Landau, 2013).

In the tropics, regional, continental or pantropical models are frequently employed for H estimation. One of the widely used pantropical H:D models was developed by Chave et al. (2014), where H is predicted from D and three climatic variables. This model was constructed using a dataset comprising 4004 trees from 58 sites encompassing tropical forests, subtropical forests and woodland savannas. Most databases used for pantropical allometries combine D and H data collected at permanent plots using various inventory methods, each with distinct measurement uncertainties (Burt et al., 2020). Even when H is measured destructively, often different approaches are applied post-harvest (Burt et al., 2020). The accuracy of H measurements is also contingent on the structural complexity of the forest, the observer's experience and the equipment employed. This can introduce subjectivity and measurement heterogeneity, potentially biasing the resulting H:D models (Laurin et al., 2019). Measuring D is also often challenging in tropical rainforests due to stem deformities and buttressed roots reaching several metres in height. Measuring D above these roots is time-consuming, hazardous and difficult to replicate,

particularly in the context of monitoring (Cushman et al., 2014). As a result, the measurement of D for these buttressed trees is more prone to errors, and situations may arise where the D is not measured. Nevertheless, in contrary to H, D is more consistently measured based on a single instrument and straightforward protocols such as those provided by the Forest Global Earth Observatory (ForestGEO) network (Anderson-Teixeira et al., 2015; Condit et al., 2014). Measurement difficulties can result in biased H census data, especially for large tropical trees with substantial AGB, impacting the H:D relationships. This raises questions about the accuracy of H:D models derived from various inventory-based measurements. Specifically, data interoperability and the influence of measurement uncertainty, as well as traceability, must be well understood before utilizing these extensive global databases to establish new allometries.

Terrestrial laser scanning (TLS), also known as terrestrial lidar, has transformed the way we assess forest structure. Laser scanning is an active remote sensing technique that emits laser pulses and analyses the returned energy over time (in the case of time-of-flight scanners) or the phase difference (in case of phase-shift scanners) to precisely measure distances. With this technology, we can capture the three-dimensional (3D) structure of the forest and its individual trees in the form of point clouds. These point clouds allow us to derive structural metrics like D, H and crown dimensions relatively quickly, accurately and easily (Calders et al., 2015; Hopkinson et al., 2004; Tansey et al., 2009). A study conducted by Terryn et al. (2022) demonstrated that using high-end TLS equipment (RIEGL VZ400), accuracies of 2 cm for D (at both breast height and above buttresses) and 30 cm for H can be achieved for trees (15–37 m tall) in two dense tropical rainforest plots. In contrast, inventory-based H measurements in dense tropical forests can exhibit biases of up to 10 m (Laurin et al., 2019). Over recent years, the use of TLS in forest assessments has witnessed a substantial rise, establishing itself as a traceable, non-destructive and accurate method for numerous tree structural measurements. However, it is crucial to highlight that achieving this is feasible only after processing the raw point cloud data, which essentially comprises *x*, *y*, *z* coordinates. Processing steps, such as co-registration and tree segmentation, particularly the latter, can be quite time-consuming. Fortunately, laser scanning data for trees are increasingly accessible to the public through platforms such as GlobalTLS (https://www.global-tls.net/), ForestScan (https://data.ceda.ac.uk/neodc/forestscan), and FOR-instance (Puliti et al., 2023). This development opens up new opportunities for the evaluation and improvement of existing H:D models based on highly accurate 3D tree measurements.

In this study, we compiled a comprehensive dataset of highly precise D and H measurements acquired through TLS. This dataset encompasses 1951 trees across 19 distinct tropical rainforest plots across four different continents. Our investigation focuses on two main research questions: First, what is the predictive accuracy of forest inventory-based local H:D allometries in tropical rainforests? To address this, we utilized spatially coincident TLS-based and forest inventory-based H and D data available for 11 of the 19 plots. Second, can we decrease the uncertainty and bias of pantropical H:D allometries using TLS? To explore this, we developed a new H:D model for tropical rainforests, leveraging TLS-based H and D data from all 19 plots. Our research highlights the importance of quantifying prediction uncertainty stemming from H measurement errors at both local and pantropical scales. It illuminates the impact of forest inventory height measurement errors on H:D allometries and the potential of TLS for mitigating those errors.

2 | MATERIALS AND METHODS

2.1 | Data

2.1.1 | Terrestrial laser scanning

We compiled a pantropical dataset comprising 1951 point clouds of tropical rainforest trees, which had been previously extracted from TLS data as part of earlier studies. The dataset spans 19 different tropical rainforest plots from 10 different countries (Figure 1, Table 1). Precipitation at these plots ranges from approximately 1800 to 3500 mm per year according to the WorldClim database (0.5′ resolution) (Fick & Hijmans, 2017). We selected a D cut-off of 10 cm since this is a frequently selected cut-off point in inventory measurements in tropical rainforests (Harris et al., 2021). All TLS data were collected with a RIEGL VZ-400 or VZ-400i TLS instrument for data interoperability (Calders et al., 2017). Both of these systems are full waveform, multiple target instruments with similar scanner characteristics. More specifications on TLS data collection for each plot can be found in Table S1.

Tree point clouds were segmented from the co-registered plot point cloud either completely manually or with a combination of a segmentation algorithm and manual corrections afterwards to ensure a high-quality dataset (Table S1). The sampling strategy of individual trees differed between plots as the trees were extracted in the context of different research projects for which these data were initially collected (Table S1). D and H were calculated from the tree point clouds with the ITSMe package in R (Terryn et al., 2023). The parameters for the D calculation were optimised for each plot and a visual inspection of the calculation through figures, such as Figure S1, ensured the D estimates' quality.

2.1.2 | Forest inventory

For 11 of the 19 plots, inventory data of the same plot as the TLS data was gathered either from publicly available sources such as the Tallo database (Jucker et al., 2022) or unpublished sources (Table S1). If inventory data were available from multiple years, the year closest to when the TLS data were collected was chosen (Table 1). The inventory-based H measurements varied from using measuring tape for small trees, clinometers and laser rangefinders to using ground-based Field-Map technology (IFER, Ltd.) and canopy cranes for

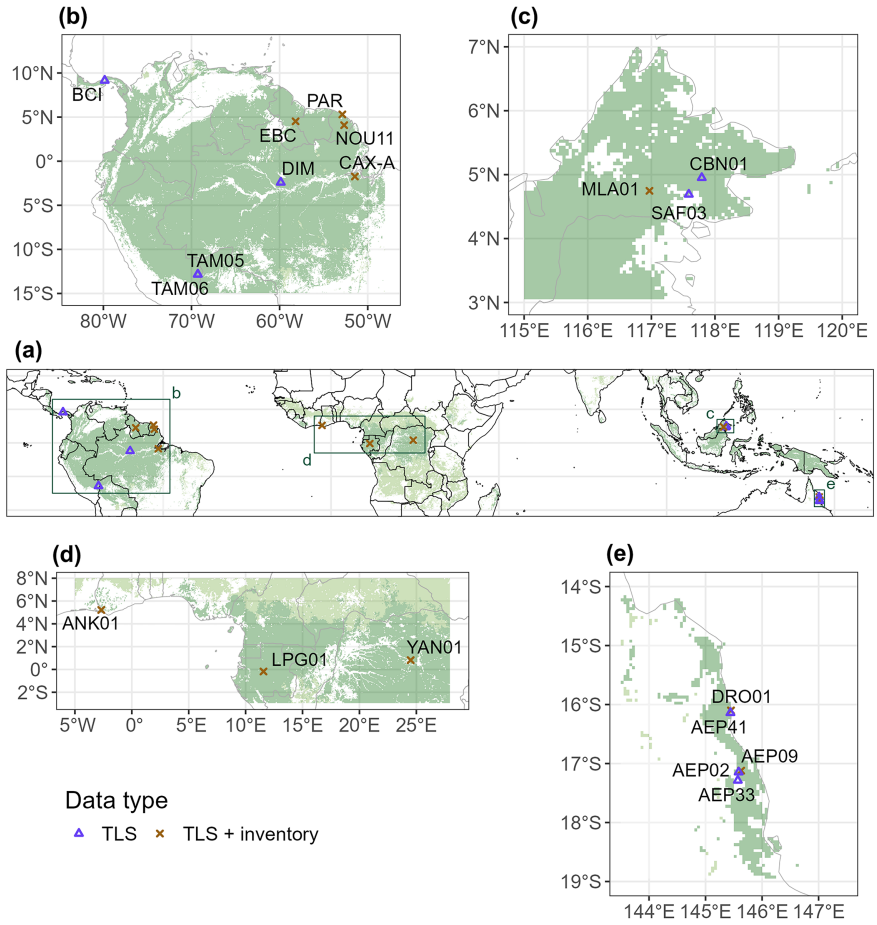

FIGURE 1 Spatial coverage of the terrestrial laser scanning (TLS) and forest inventory (inventory) data that include tree height measurements of tropical rainforests (a) pantropical and in (b) South America, (c) Asia, (d) Africa and (e) Australia. TLS data of all 19 plots were used in the pantropical allometry analysis. Coincident TLS and inventory data of 11 plots (marked by a brown cross) were used in the local allometry analysis. Dark and light green colours on the map show evergreen and deciduous forests, respectively (ESA's Global Land Cover Map of 2020). Map lines delineate study areas and do not necessarily depict accepted national boundaries.

canopy trees (Table S1). For the EBC plot, in addition to TLS-based and inventory-based H and D measurements, post-harvest measurements were available, providing insight into how well TLS-based H:D allometry compares to post-harvest-based (destructive) H:D allometry (Lau et al., 2019).

2.1.3 | Environmental variable

To build our new pantropical H:D model for tropical rainforests, we chose to add the maximum climatological water deficit (MCWD) to the model. The MCWD is a measure of the severity of water stress that vegetation may experience during a certain period. The MCWD has proven to be a key environmental variable in pantropical models before and is highly correlated (correlation >0.8) with other environmental variables, temperature seasonality, precipitation seasonality and dry season length, that were found to drive the H:D allometry of tropical trees (Banin et al., 2012; Chave et al., 2014; Feldpausch et al., 2011). Given the constraints of our study, which is confined to 19 tropical rainforest plots, we opted to include just one environmental variable (MCWD) to prevent overfitting. This decision not only addresses overfitting concerns but also ensures the interpretability of the model. The MCWD, calculated as the mean yearly MCWD over a period of 1981 to 2020, was extracted from the Global CHIRPS MCWD (Maximum Cumulative Water Deficit) Dataset (Funk et al., 2015; Silva Junior et al., 2019; Silva Junior et al., 2021).

2.2 | Local H:D allometry analysis

To assess the prediction accuracy of plot-level inventory-based H:D allometries, we compare them to H:D allometries build on the best available data (TLS) for that plot. Therefore, we constructed fixed effect models for each plot, incorporating the data type (TLS, inventory or post-harvest for EBC) as a fixed effect across all potential combinations of model parameters (Figure S2, Equations 1–4; Equations S1).

2.2.1 | Plot selection

In an ideal scenario, we would have spatially and temporally coincident TLS and inventory data for the same trees within each plot. This approach would eliminate the influence of plot environment, temporal changes and differences in sampling strategies on the results. This requires, first and foremost, that TLS and inventory height (H) and diameter (D) data from the same year are available for the same plot. Additionally, it requires matching individual trees from TLS data to inventory data.

TABLE 1 Summary of the assembled terrestrial laser scanning (TLS) and forest inventory (inventory) data including plot code, the country where the plot is located (international country code), the year of data collection (TLS/inventory), the number of trees (TLS/inventory/post-harvest) used in the local H:D allometry analysis (LAA), the number of trees (TLS) used in the pantropical allometry analysis (PAA, total number of 1951), the stem diameter (D) range, the tree height (H) range of the trees for the pantropical allometry analysis and the maximum climatological water deficit (MCWD).

Plot code	Country	Collection year	# trees LAA	# trees PAA	D range (cm)	H range (m)	MCWD (mm)
EBC*	GUY	2017/2017	26/26/26	106	10–157	14–52	−131
LPG01	GAB	2013/2013	104/106	107	19–223	15–43	−287
YAN01*	COD	2023/2023	110/110	106	10–76	10–43	−62
AEP09*	AUS	2018/2019	57/57	200	12–90	19–38	−373
DRO01*	AUS	2018/2019	56/56	59	15–123	10–35	−352
ANK01	GHA	2016/2015	179/66	182	11–101	12–40	−195
MLA01	MYS	2018/2014	189/402	189	10–149	10–77	−18
PAR06	GUF	2019/2012	204/499	202	10–93	15–45	−148
BCI	PAN	2019/2014	195/339	196	22–211	17–43	−222
CAXA	BRA	2014/2023	151/496	151	11–160	21–56	−156
NOU11	GUF	2015/2005	155/214	155	19–105	17–52	−69
AEP02	AUS	2018/–	-	27	18–45	13–23	−410
AEP33	AUS	2018/–	-	16	50–100	28–41	−395
AEP41	AUS	2018/–	-	32	10–72	15–33	−385
CBN01	MYS	2017/–	-	44	10–111	10–52	−18
DIM	BRA	2021/–	-	83	10–75	12–36	−42
SAF03	MYS	2018/–	-	35	12–92	9–44	−24
TAM05	PER	2017/–	-	37	15–117	13–42	−144
TAM06	PER	2017/–	-	24	17–89	12–37	−145

*For these plots, the individual trees in the TLS and the inventory data were paired. The relative D and H distribution of TLS and inventory-based data for each plot used in the LAA are shown in Figure S3.

For two plots (YAN01 and EBC), we obtained matched tree data from the same year and plot (Table 1). For two other plots (DRO01 and AEP09), matched TLS and inventory data were available but collected 1 year apart. Matching between the TLS and inventory tree data was done manually for these plots. For YAN01, trees were first segmented from the TLS data, and a map with tree locations was created. This map was later used to locate trees in the field to measure their diameter D and H using inventory methods. For EBC, individual trees were selected, conventionally measured, scanned and harvested (Lau et al., 2019). For DRO01 and AEP09, reflective QR codes attached to the trees during scanning were used to identify the trees during tree segmentation (Terryn et al., 2022).

For seven other plots (LPG01, ANK01, MAL01, PAR06, CAXA, NOU11 and BCI), both TLS-based and inventory-based H and D data were available, but tree matching was not possible. Furthermore, for five of these plots, there is a time gap of more than 1 year (up to 10 years) between the TLS and inventory data collection (see Table 1). Since tree matching was not feasible, we ensured that for each of these seven plots, there were at least 50 individuals in both datasets (TLS and inventory). Sullivan et al. (2018) suggested a sample size of at least 50 trees (including the 10 largest) per plot to achieve local allometries with low prediction error.

2.2.2 | Model forms, fitting and selection

First, the TLS, post-harvest and inventory datasets were combined for each plot. To fit the allometric models for plots where tree matching was not feasible, we used all available trees from TLS and inventory data that fell within a comparable diameter range. For example, if the minimum diameter (D) for inventory data was 10 cm but 18 cm for TLS, we included only trees with a D greater than 18 cm. For the maximum diameter, we set the cut-off where the difference between the maximum diameters for TLS and inventory data was less than 10 cm.

For model fitting, we considered four commonly used functional forms to model the local H:D relationships, namely the log–log form (Equations 1), the log–log^2 form (Equation 2), the rescaled Weibull form (rWei, Equation 3) and the generalised Michaelis–Menten form (gMM, Equation 4). The latter two are non-linear H:D models, having biological interpretations, that are less sensitive to individual points, making them more stable and more reliable for data extrapolation (Batista et al., 2001). We applied a natural logarithm transformation on the rescaled Weibull, and the generalised Michaelis–Menten form to increase the likelihood of homoscedastic behaviour of the residuals:

$$\ln(H) = a + b \cdot \ln(D) + \epsilon, \quad (1)$$

$$\ln(H) = a + b \cdot \ln(D) + c \cdot \ln(D)^2 + \epsilon, \quad (2)$$

$$\ln(H) = a + \ln\left(1 - \exp\left(-b \cdot D^k\right)\right) + \epsilon, \quad (3)$$

$$\ln(H) = a + b \cdot \ln(D) - \ln\left(k + D^b\right) + \epsilon, \quad (4)$$

with H, the tree height in metres, D, the stem diameter in centimetres, a, the intercept and b, c and k, the shape parameters of the functional forms, ε the error term, ln the natural logarithm and exp the exponential function.

Fixed effect models were fitted with the data type (e.g. the method of H and D measurements: TLS, inventory, post-harvest) treated as a fixed effect factor on the intercept and shape parameters. By including data type as a fixed effect on these parameters, we accounted for the variation in the H and D relationship that may arise from different data types used to fit the allometry. Since it is unclear which parameters might be influenced by the data type, we explored different combinations of adding data type as a fixed effect to the parameters of the four different model forms. Hence, for each functional form, we fit a null model with no fixed effect of the data type (Equations 1–4), as well as 24 models incorporating each possible combination of fixed effects of the data type on the intercept and the shape parameters (Equations S1).

To fit the H:D allometries, we used Bayesian multilevel models implemented by the brms R package (version 2.19.0), which uses the probabilistic programming language Stan (Bürkner, 2017). Priors for the a, b, c and k parameters were based on previous literature (Chave et al., 2014; Feldpausch et al., 2011; Martnez Cano et al., 2019), and modelled as normal distributions and in case of rWei and gMM models as gamma distributions. The utilization of gamma distributions aimed to enhance model convergence by ensuring that all parameters remain positive. The fixed effects priors were modelled as zero-centred uninformed normal distributions. Model inference relied on drawing 5000 posterior samples after conducting a burn-in of 10,000 iterations across four parallel chains to guarantee model convergence while limiting computing time. Trace, density and post-predictive check plots (Figures S4, S5), along with the Gelman–Rubin Statistic (R-hat) and effective sample size (ESS) were employed to verify and ensure model convergence and model structure. For each plot, the best model was selected based on the Bayesian leave-one-out (LOO) cross-validation method using the *loo* and *loo_compare* function within the brms package (Luo & Al-Harbi, 2017; Sivula et al., 2020).

2.3 | TLS-based pantropical H:D allometry analysis

To improve the estimation of H on a pantropical level, we built a new pantropical H:D model using mixed-effect models. This model was based on TLS-based H and D, from 1951 tree point clouds from tropical rainforests across four continents, and the MCWD to help account for between plot variance (Figure S6).

2.3.1 | Model forms, fitting and selection

We also applied Bayesian models implemented by the brms R package to fit the mixed-effect pantropical H:D models (Bürkner, 2017). First, we explored the fit of the same model forms (Equations 1–4) as were applied for the local allometry analysis to the full TLS dataset, to obtain pantropical H:D allometries for each model form. These allometries do not yet consider any environmental factors but we did account for between-plot variation using 'plot' as a random factor in the models. Adding a random effect for plot helps to account for the nested structure in the data. Random effects can capture the variation in H:D relationship between the different plots. For each functional form for the simple pantropical H:D allometries, eight different combinations of random effects (including no random effects) on the model parameters a, b, c or k were added to account for plot grouping, resulting in 28 different models (Equations 1–4; Equations S25–S47). For all models, inference was based on 5000 posterior samples following 10,000 burn-in iterations for four parallel chains to guarantee model convergence while limiting computing time. Trace, density and post-predictive check plots (Figures S4, S5), along with the Gelman-Rubin Statistic (R-hat) and ESS were employed to verify and ensure model convergence and model structure. The best model among the 28 different models was determined based on the LOO comparison method and is further referred to as the simple pantropical model as it does not include any environmental variables.

Secondly, the model form selected for our simple H:D allometry (excluding the environmental variable MCWD) served as the foundation for further model development. This was done to create a complex pantropical H:D model that incorporates MCWD to address between-plot variance. MCWD was introduced to the model parameters where the simple pantropical model exhibited a random effect of plot, indicating variance between plots. The random effects were also included because even if a model includes and accounts for a number of explanatory variables, other unaccounted effects could still play a role on the response variable. Hence, the combined effect of these possible omitted variables can still be represented by the random effects (Cysneiros et al., 2021).

2.4 | Accuracy and trueness assessment

To assess the difference in local inventory-based and TLS-based H:D allometries, we applied the best model (see Local H:D allometry analysis section, Table 2) to make predictions of H for the D range, assuming TLS and inventory data as the data type, for each plot. The predicted heights were corrected for the bias introduced by the back transformation of the log-transformed predictions (Martnez Cano et al., 2019). Next, we calculated the absolute height differences ($\hat{H}_{\text{inventory}} - \hat{H}_{\text{TLS}}$) and relative height differences ($\hat{H}_{\text{inventory}} / \hat{H}_{\text{TLS}} - 1$). We computed 95% credible intervals (CI) based on 5000 samples from the posterior distributions of all parameters of the corresponding allometric models. The CI means that there is

TABLE 2 Summary table of the best model for each plot, specifying its model form, the estimates and the 95% credible interval (CI) of the intercept (*a*) and the shape parameters of the functional forms (*b*, *c* and *k*), the estimates and the 95% CI of the fixed effects of data type on these parameters, and the root mean square error (RMSE, [m]) of the model.

Plot code	Model form	Parameter	Parameter estimate	Estimate 95% CI	Fixed effect estimate	Estimate 95% CI	RMSE
EBC	gMM	*a*	3.98	[3.86, 4.14]	-	-	0.11
		b	1.00	[0.86, 1.13]	−0.08	[−0.13, −0.04]	
		k	25.43	[20.92, 30.39]	-	-	
LPG01	log–log	*a*	1.68	[1.36, 2.00]	−0.59	[−1.04, −0.13]	0.21
		b	0.43	[0.34, 0.51]	0.17	[0.04, 0.29]	
YAN01	rWei	*a*	3.70	[3.47, 4.01]	−0.23	[−0.65, 0.34]	0.19
		b	0.06	[0.05, 0.08]	-	-	
		k	0.78	[0.65, 0.93]	0.05	[−0.21, 0.27]	
AEP09	log–log^2	*a*	1.48	[1.09, 1.86]	-	-	0.12
		b	0.66	[0.46, 0.86]	-	-	
		c	−0.04	[−0.07, −0.02]	-	-	
DRO01	log–log^2	*a*	1.16	[0.71, 1.60]	-	-	0.23
		b	0.69	[0.49, 0.91]	-	-	
		c	−0.04	[−0.07, −0.01]	-	-	
ANK01	rWei	*a*	3.65	[3.54, 3.81]	-	-	0.18
		b	0.05	[0.03, 0.07]	−0.03	[−0.05, −0.01]	
		k	0.91	[0.75, 1.08]	0.23	[0.02, 0.44]	
MLA01	log–log^2	*a*	0.63	[0.29, 0.96]	−1.39	[−2.00, −0.78]	0.22
		b	0.93	[0.74, 1.12]	0.80	[0.44, 1.17]	
		c	−0.04	[−0.07, −0.01]	−0.13	[−0.18, −0.07]	
PAR06	rWei	*a*	3.63	[3.55, 3.73]	-	-	0.16
		b	0.07	[0.06, 0.08]	−0.01	[−0.02, −0.01]	
		k	0.86	[0.78, 0.95]	-	-	
BCI	log–log^2	*a*	0.90	[0.44, 1.37]	−1.78	[−2.81, −0.77]	0.16
		b	0.80	[0.59, 1.01]	0.84	[0.34, 1.37]	
		c	−0.04	[−0.07, −0.02]	−0.10	[−0.17, −0.04]	
CAXA	log–log^2	*a*	1.29	[0.83, 1.74]	−1.56	[−2.25, −0.85]	0.25
		b	0.75	[0.54, 0.96]	0.57	[0.17, 0.97]	
		c	−0.05	[−0.07; −0.02]	−0.06	[−0.12, −0.00]	
NOU11	rWei	*a*	4.05	[3.80, 4.54]	−0.36	[−0.89, 0.08]	0.15
		b	0.07	[0.04, 0.10]	−0.04	[−0.07, −0.00]	
		k	0.73	[0.51, 0.97]	0.30	[−0.07, 0.66]	

Note: The value for the fixed effect equals the increase/decrease (when +/−) in the model parameter when the allometric model is modelled using inventory compared with TLS (the reference data type) tree heights.

a 95% probability that the true (unknown) estimate would lie within the interval, given the evidence provided by the observed data.

We also assessed model prediction accuracy, the closeness between the predicted and observed H, and the trueness, the part of accuracy related to systematic errors, of the inventory local H:D allometries, and the simple and complex pantropical TLS-based H:D allometries. To assess prediction error, we used a relative accuracy metric, the natural logarithm of the accuracy ratio (Tofallis, 2015) instead of the mean absolute percentage error (MAPE). As Burt et al. (2020) pointed out, MAPE has undesirable properties including asymmetric penalty, asymmetric bounds and outlier penalty. The natural logarithm of the accuracy ratio Q_i is defined as the natural logarithm of the ratio of the estimated $\left(\hat{H}_i\right)$ and the measured H $\left(H_i\right)$:

$$\ln\left(Q_i\right) = \ln\left(\frac{\hat{H}_i}{H_i}\right). \quad (5)$$

For the local inventory H:D allometries, for each plot we applied the best model to make predictions of H for all TLS trees using the inventory H:D allometry $\left(\hat{H}_i = \hat{H}_{\text{inventory}}\right)$ and the TLS-based H as a reference $\left(H_i = H_{\text{TLS}}\right)$. For the pantropical H:D allometries, we assessed model

prediction accuracy and trueness of the simple and complex pantropical model using k-fold cross-validation. We used the *kfold* function of the brms R package to perform 19-fold cross-validation by refitting the selected model 19 times each time leaving out one plot of the original data (Bürkner, 2017). Subsequently, the *kfold_predict* function of the same package was applied to compute the H predictions considering no group-level effect (similar to predicting H for new plots).

We quantified the accuracy (uncertainty) of the H estimations using the median symmetric accuracy (MSA, Morley et al., 2018). The value of MSA can be interpreted as a percentage total error (e.g. a value of 10% means a total error of 10%) and is calculated as

$$\mathrm{MSA} = 100 \cdot \left(\exp\left(M\left(\left|\ln(Q_i)\right|\right) - 1\right)\right), \tag{6}$$

with M representing the median function. We also quantified the trueness (bias) using the systematic signed percentage bias (SSPB, Morley et al. (2018)), which gives the percentage systematic error (e.g. a negative percentage value of −10% means a 10% negative bias and a positive percentage value of 10% means a 10% positive bias):

$$\mathrm{SSPB} = 100 \cdot \left(\mathrm{sgn}(M(\ln(Q_i))) \cdot \exp(M(\ln(Q_i))) - 1\right), \tag{7}$$

with sgn representing the sign function and M representing the median function. In comparison with existing H:D models, we also calculated the MSA and SSPB for the H predictions based on the pantropical H:D model of Chave et al. (2014) (equation 6a–6b).

3 | RESULTS

3.1 | Local H:D allometry

Our analysis shows that for all plots, apart from two (AEP09 and DRO01), the best local H:D model included fixed effects of data type on one or several parameters (Table 2). Notably, for two of those plots (ANK01, LPG01) this does not result in statistically credible (95% CI, in the Bayesian sense) differences between inventory-based and TLS-based allometries over the full D range (Figure 2). Conversely, for seven plots, the inventory-based allometries exhibit statistically credible underestimation (95% CI) of H, with mean values between −1.62 m (−5.32%) and −7.52 m (−25.42%) for trees of 30 m tall (Figure 3; Figure S7). For the Malaysian plot (MLA01) the underestimation increases up to −31.70 m (−41.26%) for the tallest trees (Figure 3, bottom). In the majority of plots, the underestimation of H is not consistent across the height range; it increases with H for certain plots but decreases for others. In contrary to all other plots, for the LPG01 plot, H is overestimated for trees taller than approximately 25 m (Figure 3). The H difference is also often accompanied by an increase in the width of the CI with increasing H (Figure 3). The widening of the CI with tree size is caused by the limited number of trees with high H values which increases the uncertainty of the allometric models at these tree sizes.

For EBC, the only plot where coincident TLS, post-harvest and inventory data of the same trees was available, the best H:D model shows overlapping fits for TLS and post-harvest whereas the fit for inventory allometry did not overlap and was credibly (95% CI) lower (Figure 2). Compared with the TLS allometry, the allometry based on this inventory data (using a laser rangefinder) underestimates H on average between −2.50 m (−6.2%) and −3.52 m (−12%) along the diameter range (Figure 3).

3.2 | TLS-based pantropical H:D allometry

We found the best allometric form, for our simple pantropical H:D model (excluding environmental variables), to be the log–log^2 form (Equation 2) with random effects of plot on parameters a and b:

$$\ln(H) = (a|\ \mathrm{plot}) + (b|\ \mathrm{plot}) \cdot \ln(D) - c \cdot \ln(D)^2 + \epsilon, \tag{8}$$

with H, the tree height in metres, D, the stem diameter in centimetres, a, b and c model parameters, ϵ the error term, and ln the natural logarithm. Fitting this form (Equation 8) to the TLS data resulted in our best-fit simple pantropical H:D model:

$$\ln(H) = \left(0.91 + a_{\mathrm{plot}}\right) + \left(0.86 + b_{\mathrm{plot}}\right) \cdot \ln(D) - 0.06 \cdot \ln(D)^2, \tag{9}$$

with $a_{plot} \sim \mathcal{N}\left(0, 0.38^2\right)$ the random effect of plot on the intercept a and $b_{plot} \sim \mathcal{N}\left(0, 0.10^2\right)$ the random effect of plot on the shape parameter b (Table 3; Figure S8). The model has a mean uncertainty (MSA, total error) of 19.70% and a mean bias (SSPB, systematic error) of −4.78% based on cross-validation (Table 4).

To account for between plot variation, we added the MCWD to the parameters a and b of the simple pantropical H:D allometry form:

$$\ln(H) = (a|\ \mathrm{plot}) + e \cdot MCWD + ((b|\ \mathrm{plot}) + f \cdot MCWD) \cdot \ln(D) - c\ln(D)^2 + \epsilon, \tag{10}$$

where e and f are additional model parameters compared with the simple pantropical H:D model form and MCWD is the maximum climatological water deficit (mm). Fitting this form (Equation 10) to the data resulted in our best-fit complex pantropical H:D model:

$$\ln(H) = \left(0.76 + a_{\mathrm{plot}}\right) - 1.22 \cdot MCWD + \left(\left(0.93 + b_{\mathrm{plot}}\right) + 0.56 \cdot MCWD\right) \cdot \ln(D) - 0.05 \cdot \ln(D)^2, \tag{11}$$

with $a_{plot} \sim \mathcal{N}\left(0, 0.32^2\right)$ the random effect of plot on the intercept a and $b_{plot} \sim \mathcal{N}\left(0, 0.07^2\right)$ the random effect of plot on the shape parameter b (Table 3; Figure S8). Adding the MCWD to the model has reduced the standard deviation of the random effects on a and b compared with the simple pantropical model (Equation 9). This suggests that MCWD accounts for some of the between plot variance but not all of it. This model has a mean uncertainty (MSA, total error) of 19.14% and a mean bias (SSPB, systematic error) of −4.77% based on cross-validation (Table 4).

Compared with the model of Chave et al. (2014) and the simple pantropical model (Equation 9), the mean uncertainty of the complex pantropical model (Equation 11) is lower and uncertainties are more stabilised along all tree heights (Figure 4). Moreover, looking at the different height classes, the mean bias for trees taller than 40 m in the complex pantropical model is also lower (Figure 4). Interesting to

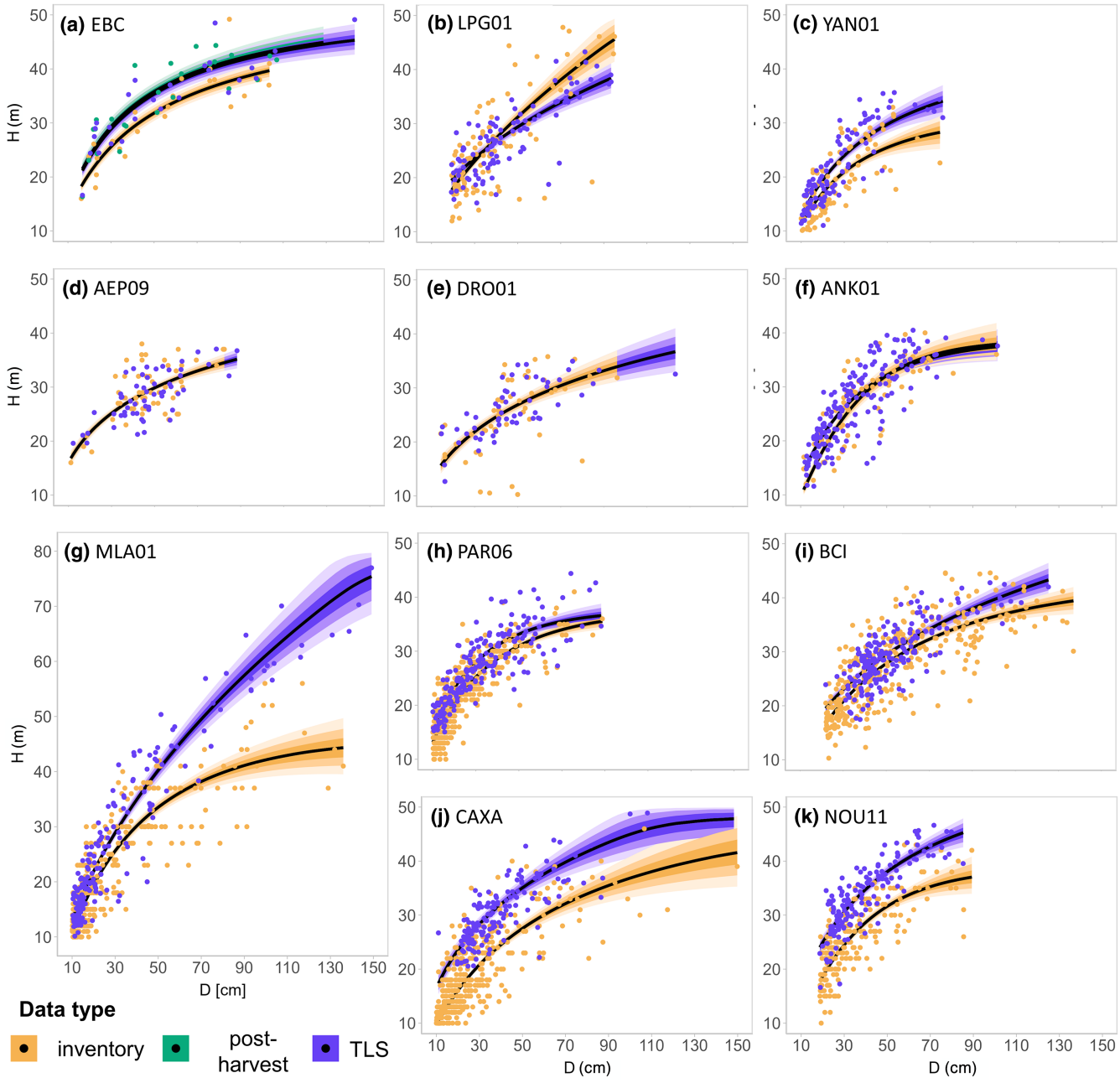

FIGURE 2 Best tree height:stem diameter (H:D) model fit for each plot (a–k). The model fits for forest inventory (inventory), terrestrial laser scanning (TLS) and post-harvest tree height (H) and stem diameter (D) data are shown in black lines with orange, purple and green credible intervals (CI) respectively. The 0.95, 0.8 and 0.5 CI are shown in different shades going from dark to light respectively. The individual trees are represented as dots in the same colours. There is some binning visible in the inventory H data for some plots due to the limited precision (1 m) of those H measurements.

note is the very low bias of the Chave et al. (2014) model for trees smaller than 20 m. Most of the trees (1766, 60%) used to calibrate Chave et al. (2014) their model were less than 20 m tall.

The comparison of the uncertainty and bias between local inventory-based and the complex pantropical TLS-based H:D model shows that for the majority of the plots the mean uncertainty (MSA) is lower for the local inventory-based models than the complex pantropical model (Figure 5). Conversely, for mean bias (SSPB), the complex pantropical model demonstrates lower values compared with the local inventory-based models in the majority of the plots.

3.3 | TLS versus forest inventory dataset comparison

Our TLS dataset of tropical rainforest trees exhibits an inherently different tree size distribution compared with typical inventory

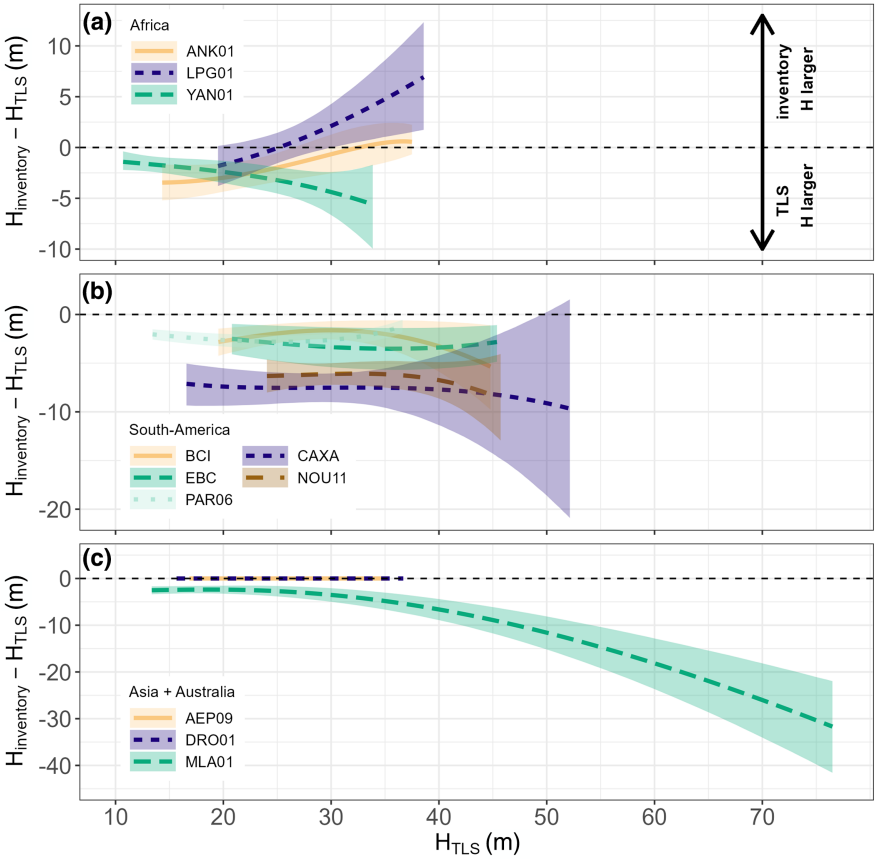

FIGURE 3 Absolute difference in tree height (H) when predicted from the best allometry for forest inventory (inventory) data versus terrestrial laser scanning (TLS) data (i.e. $H_{inventory} - H_{TLS}$) for plots in (a) Africa, (b) South America and (c) Asia and Australia. Negative values indicate that the inventory allometry underestimates the tree height compared with the TLS-based allometry. The different colours and line types reflect the different plots per panel and the shaded area is the 0.95 credible interval (CI). The same figure but for relative tree height difference can be found in Figure S7.

TABLE 3 Summary table of the best model for the simple (Equation 9) and complex pantropical model (Equation 11), specifying the estimates for the model parameters and σ (the standard deviation of ϵ) and the 95% credible intervals (CIs) on these estimates, and also the estimate of the standard deviation of the random effect on a and b and their 95% CIs.

H:D model	Parameter	Parameter estimate	Estimate 95% CI	Standard deviation random effect estimate	Estimate 95% CI
Simple pantropical	a	0.91	[0.64, 1.2]	0.38	[0.26, 0.56]
	b	0.86	[0.72, 0.98]	0.10	[0.07, 0.15]
	c	−0.06	[−0.07, −0.04]	-	-
	σ	0.14	[0.13, 0.14]	-	-
Complex pantropical	a	0.76	[0.45, 1.09]	0.32	[0.21, 0.49]
	b	0.93	[0.80, 0.1.06]	0.07	[0.05, 0.11]
	c	−0.05	[−0.07, −0.04]	-	-
	e	−1.22	[−2.24, −0.12]	-	-
	f	0.56	[0.26, 0.84]	-	-
	σ	0.14	[0.13, 0.14]	-	-

datasets used for modelling H:D allometry, such as those utilized by Chave et al. (2014) and the Tallo database by Jucker et al. (2022) (Figure S9). Our TLS dataset contains only 66% and 1% of the number of tropical rainforest trees compared with Chave et al. (2014) and the Tallo dataset, respectively. But, compared with the Tallo database, this percentage increases to 3% and 4% when considering D above 20 and 40 cm, respectively. Moreover, compared with Chave et al. (2014), our TLS dataset contains proportionally 34.5%, and 75.1% more trees with a D above 20 cm and 40 cm, respectively. Thus, these inventory datasets exhibit a relative underrepresentation of larger trees compared with TLS.

All the trees from the TLS dataset were measured with the same H measurement method, while Burt et al. (2020) reported that at least four different methods (pre- and post-harvest) were used in the dataset Chave et al. (2014) compiled. Also for the Tallo database, Jucker et al. (2022) report that tree heights were measured using a variety of approaches, including laser or ultrasonic range finders, clinometers, as well as tape measures, telescopic

TABLE 4 Results of the cross-validation prediction metrics for pantropical H:D allometries: Pantropical model of Chave et al. (2014) equation 6a–6b, the simple pantropical model (Equation 9) and complex pantropical model (Equation 11).

H:D model	Mean MSA (%)	95% CI MSA (%)	Mean SSPB (%)	95% CI SSPB (%)
Chave et al. (2014)	16.88	-	−13.00	-
Simple pantropical	19.70	[16.58, 23.90]	−4.78	[−12.31, 2.49]
Complex pantropical	19.14	[16.17, 23.35]	−4.77	[−12.24, 2.45]

Notes: The median symmetric accuracy (MSA) and the systematic signed percentage bias (SSPB) quantify the uncertainty (total error) and bias (systematic error) respectively. The mean MSA and SSPB values and their 95% credible intervals (CIs) are given, calculated based on the posterior predictions. For the pantropical model of Chave et al. (2014) the calculation of a CI was not possible.

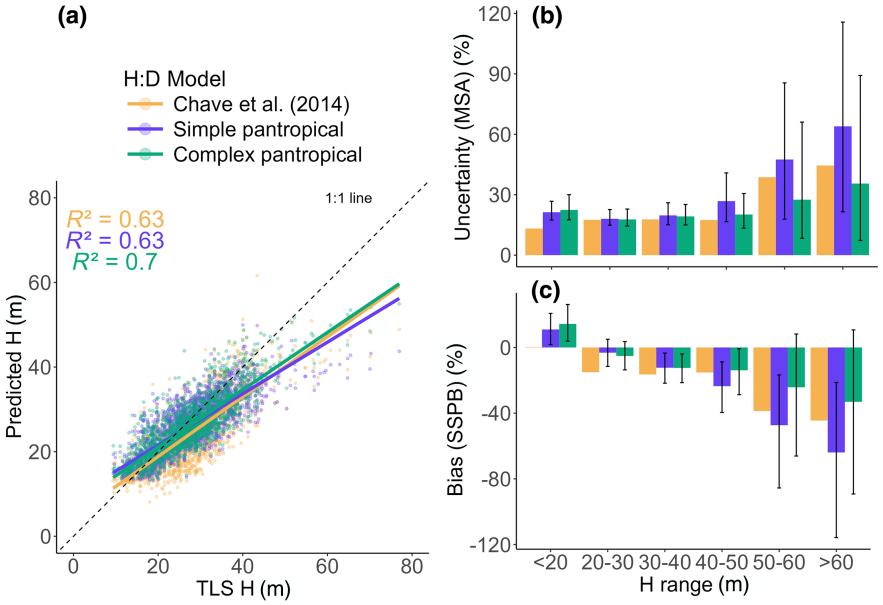

FIGURE 4 Results for the tree height (H) prediction from the pantropical H:D model of Chave et al. (2014), the TLS-based simple pantropical H:D model (Equation 9) and the TLS-based complex pantropical H:D model (Equation 11) represented in orange, purple and green respectively. (a) H predictions compared with the H measured from the terrestrial laser scanning (TLS) tree point clouds, (b) the median symmetric accuracy (MSA, [%]) quantifying the uncertainty (total error) and (c) the systematic signed percentage bias (SSPB, [%]) quantifying the bias (systematic error) of the models for different H ranges. The mean MSA and SSPB values and their 0.95 credible intervals (CIs) are given, calculated based on the posterior predictions. For the pantropical model of Chave et al. (2014), the calculation of a CI was not possible. For the TLS-based models tree height predictions were based on 19-fold cross-validation.

poles for smaller trees and for a very small subset of trees with fully sun-exposed crowns, a combination of high-resolution aerial photos and ALS.

4 | DISCUSSION

4.1 | TLS for benchmarking H

In this study, we employed TLS as a benchmark for assessing inventory-based H estimates. The accuracy of TLS-based metrics will however depend on the tree point cloud quality, which, in turn, is influenced by various factors during both acquisition and processing phases. Concerning TLS acquisition, it is important to highlight that tropical rainforests present a challenging environment, with reported instances of canopy occlusion at the canopy's uppermost layer (Schneider et al., 2019). Occlusion refers to the absence of data points in certain parts of the forest due to obstruction of the laser beams by vegetation or other obstacles in their path. Occlusion has only a minimal impact on the accuracy of H measurements as long as laser rays still hit the top of the tree which is all that is needed to get the correct H. Still a high degree of occlusion of the top of canopy can lead to underestimations of the H. The degree of occlusion within the point cloud, however, depends on a combination of several factors, including vegetation density, the specific characteristics of the laser system in use (e.g. sensor properties and scanner type) and the scanning pattern (e.g. pattern density and multi-scan approach) employed. In dense vegetation, more laser beams can be blocked by the vegetation, preventing them from reaching objects behind. However, certain laser scanner characteristics, such as a smaller laser beam divergence, greater sampling range and a higher maximum number of targets per pulse, can enhance canopy penetration. Therefore, selecting the appropriate laser scanning setup and scanning pattern

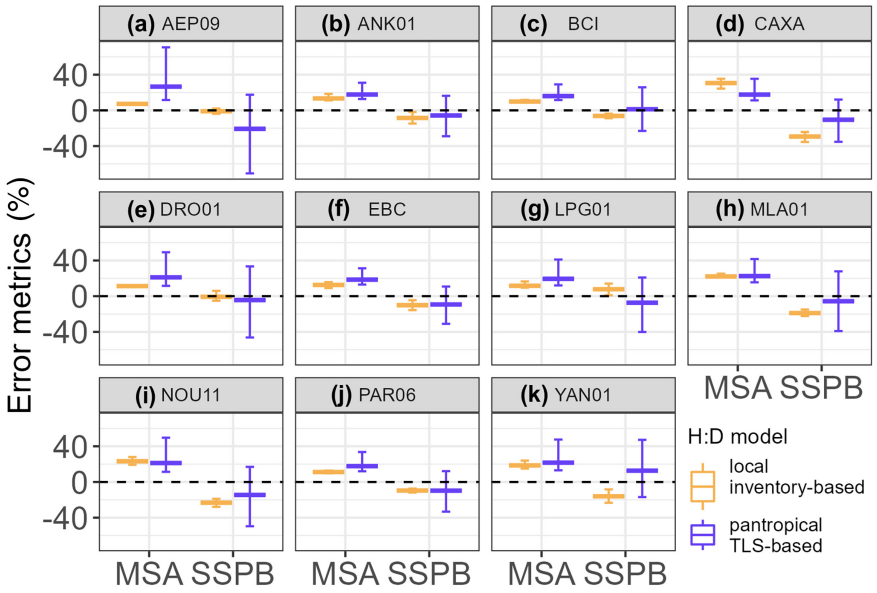

FIGURE 5 Comparison of the median symmetric accuracy (MSA, [%]) quantifying the uncertainty (total error) and the systematic signed percentage bias (SSPB, [%]) quantifying the bias (systematic error) between local forest inventory-based and the complex pantropical TLS-based H:D models (Equation 11) for each plot (a–k). The mean MSA and SSPB values and their 0.95 credible intervals (CIs) are given, calculated based on the posterior predictions based on 10-fold cross-validation.

is crucial to acquiring good-quality point clouds. Furthermore, it is important to mention that wind can induce a ghosting effect in the point cloud due to tree sway in light breezes. This could potentially impact measurements of D and H. It is therefore advisable to conduct scans when wind speeds are below 5 $m \cdot s^{-1}$ (Seidel et al., 2012; Wilkes et al., 2017). Finally, the quality of the tree point cloud also relies on the proper execution of processing steps (e.g. co-registration and tree segmentation) following data acquisition. Existing automatic segmentation algorithms exhibit limited effectiveness in tropical rainforests due to their intricate and multi-layered structure. Hence, it remains crucial to manually inspect and amend segmentation outcomes to guarantee result quality.

The tree point clouds utilized in our study were obtained using a high-quality laser scanning system employing a multi-scan approach. Additionally, manual segmentation quality checking was performed to ensure the quality of the point clouds and the structural measurements. Our findings also tend to further support the reliability of TLS-based allometries, showing no credible (95% CI) difference between TLS-based allometry and allometry derived from H measurements conducted post-harvest (destructively) in one of the plots (EBC). Consequently, TLS stands as one of the most accurate non-destructive benchmarks for H assessments, especially for tall trees in dense tropical rainforests (Ali & Wang, 2021; Ferraz et al., 2016; Gonzalez de Tanago et al., 2018; Kunz et al., 2022).

4.2 | Accuracy of forest inventory H:D allometry

Our analysis revealed that in the majority of the plots (9 out of 11), allometric models based on inventory data yielded credibly (95% CI) different H estimations compared with those constructed using TLS data. In seven of these plots, the inventory-based allometry exhibited an underestimation of H across the entire range of H. These underestimations ranged from −5.3% to −25.4% for trees measuring 30 m in height, up to −41.3% for the tallest Malaysian trees. These findings are in line with the results reported by Larjavaara and Muller-Landau (2013) for the sine method, which is often employed with laser range finders. They noted an average systematic underestimation of 20% for this method. In their study, Ojoatre et al. (2019) also observed that, in contrast to airborne laser scanning (ALS), hypsometer-measured field heights underestimated H in a tropical rainforest in Malaysia, with a RMSE of 3.11 m.

Our analysis was conducted on a limited dataset of only 11 tropical rainforest plots, with constrained replication for various inventory H measurement methods (e.g. laser range finder and clinometer). Consequently, we were unable to discern distinct patterns associated with specific inventory H measurement methods. It is interesting, however, that with plots where the same inventory H measurement method was utilized, we noticed discrepancies in the extent of underestimation. For example, while both NOU11 and ANK01 employed a clinometer for inventory H measurement, NOU11 exhibited considerable underestimation, whereas ANK01 showed no significant underestimation. This variability could be attributed to other factors, including forest structure, the individual conducting the measurement and the specific instrument used, as noted by Larjavaara and Muller-Landau (2013). Furthermore, the relationship between the accuracy and H varied from nearly constant underestimation to accuracy that decreased or even increased with increasing H. Due to this inconsistency, it is challenging to apply effective corrections on inventory H measurements. Additionally, when utilizing H data from online databases, it is often problematic to trace how and under what conditions the measurements were obtained (Burt et al., 2020). Enhancing the provision of standardized metadata during measurement publication will aid in mitigating this issue. Given the dependence of measurement accuracy on numerous factors and the traceability issues associated with inventory-based H measurements, our ability to establish reliable H:D allometries using such data is impeded.

In two plots (AEP09 and DRO01), there were no statistically significant differences (95% CI) in H between the TLS-based and inventory-based allometries, across the entire H range. Nevertheless, this does not rule out the possibility of measurement errors at the individual tree level. When comparing individual Hs for DRO01, it becomes evident that significant H differences exist at the individual tree level (see Figure 2; Figure S10a). These differences encompass both overestimations and underestimations of approximately similar magnitudes, suggesting the presence of predominantly high random errors and low systematic errors for this particular plot. In the context of allometric modelling, random errors do not result in incorrect allometries as long as a sufficient number of trees are used to model the relationship, as pointed out by Burt et al. (2020) and Sullivan et al. (2018). Conversely, systematic errors, as observed in inventory H measurements at the individual tree level in the YAN01 plot (Figure S10b), can lead to incorrect allometries.

Regrettably, in seven of the 11 plots, individual tree-level measurement errors could not be evaluated due to the lack of linkage between the tree IDs in the TLS and inventory data, often exacerbated by data collection occurring in different years. To ensure future direct comparisons, it is crucial to consistently establish connections to available census data. The absence of a link between TLS and inventory data for seven plots made it impossible to select the same trees to construct local H:D allometries. Moreover, five of these plots had a temporal difference larger than 1 year between the TLS and inventory measurements. For the unpaired plots, it is noteworthy that the differences observed between the TLS-based and inventory-based allometries may arise (partially) from this disparate tree sampling. However, concerning the difference in sample size, it primarily affects the model's uncertainty. Larger sample sizes generally result in more precise parameter estimates, with narrower credible intervals reflecting less uncertainty. Additionally, larger samples enhance the likelihood of proper model convergence due to more data informing the parameter estimates. Conversely, smaller samples may lead to convergence issues or unreliable estimates. Thus, for plots without paired data, we utilized as many available trees (for both TLS and inventory data) to build the models. Regarding the temporal differences, assuming no significant disturbances occurred during this period, the trees should follow the same H:D allometry, which would not affect our results. However, we cannot guarantee the absence of structural changes within this timeframe, so the observed differences might partially result from such changes. We acknowledge that differences in sample sizes and temporal differences could potentially influence the estimated parameters' means. Nonetheless, it is important to note that for certain sites (EBC, YAN01), we utilized the exact same trees measured in the same year, and these sites still exhibit differences. This strongly suggests that the observed differences stem from the measurement method, not sample size or sampling strategy or temporal differences.

Moreover, the absence of a link between TLS and inventory data led to a comparison of H:D allometries developed using inventory H and D data with those constructed from TLS-based H and D data. Consequently, variations in the allometries may arise not only from discrepancies in H measurements but also from differences in D measurements. It is important to note that differences in D measurements between inventory and TLS data exist, particularly for buttressed trees (Terryn et al., 2022). However, these discrepancies are considerably smaller in proportion compared with the disparities in H measurements (Figure S10), which suggests that differences between inventory and TLS allometries primarily originate from discrepancies in H measurements.

4.3 | Impact of H measurement errors from forest inventory data

Tree heights represent a crucial input for allometric equations that estimate AGB based on D and H, as outlined by Chave et al. (2014) and Feldpausch et al. (2012). A relative underestimation of H will approximately result in the same relative underestimation of tree AGB, following the AGB allometry proposed by Chave et al. (2014) (Equation 4). To illustrate using the equation of Chave et al. (2014), a 5.3% underestimation in H (which is what we obtained as a median value for trees of 30 m tall considering all plots) would correspond to an 5.2% underestimation in tree AGB for a tree of 30 m tall. However, this reasoning assumes the H data used to calibrate the AGB allometry were not biased. Burt et al. (2020) pointed out that in the case of the pantropical AGB model of Chave et al. (2014), H was predominantly measured post-felling using a tape measure, although several studies opted for pre-harvest H measurements. It is crucial to acknowledge that utilizing improved H estimations as input in AGB models, which were originally calibrated with underestimated H, could result in overestimations of AGB. Consequently, careful consideration of the calibration process for allometries based (partially) on H data, such as AGB allometries, is equally important. The impact on plot-level AGB estimation was beyond the scope of our study and would require additional species-specific information, including wood density values, and a comprehensive inventory of stem diameters within each plot. To achieve comprehensive and well-usable forest inventories in the future, it is essential to adopt standardized data collection protocols and provide adequate metadata information on the used methods. Moreover, extrapolating models to cover the entire H range could potentially lead to inaccurate estimates.

In recent years, a growing volume of inventory-based H and D data has been collected and aggregated in publicly accessible databases. Jucker et al. (2022) introduced their global tree allometry and crown architecture dataset, known as Tallo, which encompasses 498,838 georeferenced and taxonomically standardized records of individual trees, including 45% from tropical regions, with measurements of D and H. This dataset encompasses a more extensive collection of trees, including large specimens, and spans various tropical regions. Consequently, it may capture a more comprehensive spectrum of variation in H:D models compared with the dataset employed by Chave et al. (2014). Nevertheless, our findings raise important questions about the use of global databases, such as Tallo

(Jucker et al., 2022) that combine H data acquired through various methods, for constructing new pantropical H:D models before fully comprehending and rectifying the errors in these H measurements. The frequent underestimation consistently observed in our study implies that if all these inventory data were combined into a single pantropical model, this model would also likely underestimate H and subsequently lead to an underestimation of AGB when H is estimated with inventory-based allometries (Burt et al., 2020).

4.4 | TLS-based pantropical H:D allometry

We have constructed a novel pantropical H:D allometric model based on TLS data including 1951 point clouds from individual tropical rainforest trees. Despite the limited coverage of our TLS dataset, it offers consistent and precise measurements, particularly for tall trees. This is of particular significance as Sullivan et al. (2018) demonstrated that allometries with low prediction errors do not necessarily require an extensive calibration dataset but rather demand accurate and relevant data, typically 50 trees per plot, including the 10 largest specimens. Brede et al. (2022) also highlighted that only 55 individual tree samples per plot (between 1 and 4 ha) were needed to achieve a population bias of less than 5%. It is important to note that the accuracy of H measurements can be influenced by various factors, including the type of laser scanner, scanning pattern and forest structural complexity. Following rigorous field protocols can, however, help counteract or eliminate uncertainties stemming from these factors in TLS data. Nevertheless, these variables must be taken into account when integrating tree structural data from diverse TLS sources with the intention of constructing allometric models.

Our optimal pantropical H:D model adheres to the same structural form suggested by Chave et al. (2014). However, we incorporated the MCWD, which quantifies water stress and reflects hydraulic constraints on the H:D relationship. With advancements in remote sensing and climate models, MCWD data are becoming more readily available to the public. Chave et al. (2014) identified MCWD, precipitation and temperature seasonality as explanatory environmental variables for their pantropical H:D model, which encompassed tropical rainforests, subtropical forests and dryland savannas. Furthermore, our analyses unveiled that allometric models from various plots differed not only in terms of the intercept (parameter a) but also in shape (parameters *b* and *c*). In contrast to the Chave et al. (2014) model, we incorporated MCWD into both the intercept parameter (a) and one of the parameters governing the curve's shape (b). Although the inclusion of MCWD explained some of the variation between plots, a substantial amount was still unaccounted for. Numerous other factors, including species identity, forest structure, soil properties, solar radiation and presence of structural parasites have been demonstrated to influence the H:D allometry (Banin et al., 2012; Cysneiros et al., 2021; Dias et al., 2017; Feldpausch et al., 2011). Integrating more variables could potentially enhance the model, but obtaining precise pantropical data for these variables through open-access sources is not consistently feasible. It is vital to recognize that our pantropical H:D model was designed exclusively for tropical rainforests and should solely be applied to tropical rainforest trees within the calibrated D-H-MCWD range (10 cm ≤ D ≤ 223 cm, 9 m ≤ H ≤ 77 m, −410 mm ≤ MCWD ≤ −18 mm). Additionally, it is crucial to highlight that our pantropical TLS-based model was calibrated using TLS-based D measurements. As previously emphasized, TLS-based D measurements can slightly deviate from inventory D measurements, particularly in the case of buttressed trees. This discrepancy may lead to prediction errors when employing inventory D measurements as input for the TLS-based pantropical model (Burt et al., 2020). Nevertheless, given the minimal difference between inventory and TLS-based D measurements (Concordance Correlation Coefficient scores >0.96, Figure S10), especially when contrasted with the H difference, the resulting impact is expected to be limited.

In comparison with the model of Chave et al. (2014), our pantropical model exhibits an improved performance in terms of reduced uncertainty and bias for trees exceeding 20 m in height. However, for trees shorter than 20 m, our model performs less well than Chave et al. (2014). It is worth noting that the model developed by Chave et al. (2014) was primarily trained on trees below 20 m (constituting 67% of their dataset), whereas only 20% of our TLS-extracted trees were smaller than 20 m. In tropical TLS studies, the emphasis is frequently on larger trees, and not all trees within the plots undergo segmentation. This is also attributed to the substantial effort currently needed to achieve high-quality segmentation for all trees within a forest plot. Nevertheless, advancements in tree segmentation algorithms are opening avenues for achieving comprehensive segmentation (Wilkes et al., 2022). Additionally, with the raw TLS data remaining accessible, there is the potential to extract all trees, including the smaller ones, from these plot point clouds. This presents an opportunity to enhance future pantropical H:D models for the entire range of trees in the plots. Despite the better performance of the model of Chave et al. (2014) for trees below 20 m, it does not provide any insights into the error associated with H estimations, including confidence or credible intervals. Our model, akin to many others, struggles with the traditional issue of overestimation for small trees and underestimation for tall trees. In addition to the previously highlighted concern that the model may not account for other potentially influential variables affecting H, there is an additional issue where the model structure might not be aptly designed to capture the true relationship between the predictor variables (D and MCWD) and H. Burt et al. (2020) and Calders et al. (2022) have raised awareness about the use of inappropriate model forms and assumptions concerning the size dependency of allometric relationships. As a result, there is a search for new model forms utilizing dynamic allometric modelling techniques. One potential solution is the model proposed by Zhou et al. (2021). Dynamic allometric models are models that aim to depict potential size-dependent changes in the scaling between two metrics. However, it is important to note that this method is still in its initial stages concerning multivariate models.

Our findings also indicate that while local inventory-based H:D models frequently perform better in terms of uncertainty, they may exhibit worse performance in bias compared with a pantropical H:D model built on accurate TLS data. In instances where inventory H measurements are unbiased, exemplified by AEP09, the local model outperforms the pantropical H:D model significantly. However, frequently, the inventory H data exhibited bias, leading to local models that could be outperformed by the pantropical TLS-based model. The challenge lies in the unknown degree of bias present in inventory-based H data, making the decision between a local inventory-based model and a pantropical TLS-based model a complex task. Because the pantropical model was constructed based on a restricted dataset (1951 trees from 19 plots), there was a notable degree of variability in both uncertainty and bias associated with this model. Consequently, it is crucial to continuously enhance this model by incorporating more data from diverse plots that cover a broader range of environmental conditions.

5 | CONCLUSION

Tree height:stem diameter (H:D) allometries hold a critical role in the monitoring of tropical rainforest structure and the estimation and upscaling of AGB at various scales within tropical regions. However, it is important to recognize that the methodology employed for measuring H can significantly impact H:D allometries, subsequently affecting estimates and derivations based on them. Our findings reveal that in tropical rainforests, H:D allometries derived from forest inventory methods often exhibit a notable trend of underestimating H, characterized by considerable variation among different forest plots. This inherent variability complicates the task of accounting for these errors when constructing pantropical H:D models. To address this issue, we advocate for the utilization of TLS data, which offers superior accuracy and measurement consistency compared with inventory data, particularly for tall trees. In addition, we introduce a pantropical H:D model specifically tailored to tropical rainforests, constructed using TLS data from 19 diverse tropical rainforest plots spanning four continents. This model incorporates an environmental variable, the MCWD, enhancing its predictive capability. The model demonstrates stable performance with a mean uncertainty of 19.1% across various D ranges and a mean bias of −4.8%. We anticipate that these H:D model allometries will contribute to more accurate H estimates across tropical rainforests.

AUTHOR CONTRIBUTIONS

Louise Terryn: Conceptualization; data curation; formal analysis; investigation; methodology; software; validation; visualization; writing – original draft; writing – review and editing. **Kim Calders:** Conceptualization; formal analysis; funding acquisition; methodology; project administration; resources; supervision; writing – review and editing. **Félicien Meunier:** Conceptualization; formal analysis; investigation; methodology; supervision; writing – review and editing. **Marijn Bauters:** Methodology; supervision; writing – review and editing. **Pascal Boeckx:** Funding acquisition; writing – review and editing. **Benjamin Brede:** Data curation; formal analysis; funding acquisition; writing – review and editing. **Andrew Burt:** Data curation; formal analysis; funding acquisition; writing – review and editing. **Jerome Chave:** Data curation; formal analysis; funding acquisition; writing – review and editing. **Barbara D'hont:** Formal analysis; writing – review and editing. **Mathias Disney:** Data curation; formal analysis; funding acquisition; writing – review and editing. **Tommaso Jucker:** Data curation; formal analysis; funding acquisition; writing – original draft. **Alvaro Lau:** Data curation; formal analysis; funding acquisition; writing – review and editing. **Susan G. W. Laurance:** Data curation; formal analysis; funding acquisition; writing – review and editing. **Eduardo Eiji Maeda:** Data curation; formal analysis; funding acquisition; writing – review and editing. **Patrick Meir:** Supervision; writing – review and editing. **Sruthi M. Krishna Moorthy:** Data curation; formal analysis; funding acquisition; writing – review and editing. **Matheus Henrique Nunes:** Data curation; formal analysis; funding acquisition; writing – review and editing. **Alexander Shenkin:** Data curation; formal analysis; funding acquisition; writing – review and editing. **Thomas Sibret:** Data curation; formal analysis; funding acquisition; writing – review and editing. **Tom E. Verhelst:** Data curation; formal analysis; writing – review and editing. **Phil Wilkes:** Data curation; formal analysis; funding acquisition; writing – review and editing. **Hans Verbeeck:** Conceptualization; funding acquisition; methodology; project administration; supervision; writing – review and editing. **Antonio Carlos Lola da Costa:** Data curation.

AFFILIATIONS

[1]Q-ForestLab, Department of Environment, Ghent University, Ghent, Belgium
[2]ISOFYS – Isotope Bioscience Laboratory, Department of Green Chemistry and Technology, Ghent University, Ghent, Belgium
[3]GFZ German Research Centre for Geosciences, Potsdam, Germany
[4]Sylvera Ltd, London, UK
[5]Laboratoire Evolution and Biological Diversity (EDB), CNRS/IRD/UPS, Toulouse, France
[6]Geociencias, Federal University of Para, Belem, State of Para, Brazil
[7]Museu Paraense Emilio Goeldi, Belem, State of Para, Brazil
[8]UCL Department of Geography, London, UK
[9]NERC National Centre for Earth Observation (NCEO-UCL), Swindon, UK
[10]School of Biological Sciences, University of Bristol, Bristol, UK
[11]Laboratory of Geo-Information Science and Remote Sensing, Wageningen University, Wageningen, Gelderland, the Netherlands
[12]Centre for Tropical Environmental and Sustainability Science and College of Science and Engineering, James Cook University, Cairns, Australia
[13]Finnish Meteorological Institute, FMI, Helsinki, Finland
[14]Department of Geosciences and Geography, University of Helsinki, Helsinki, Finland
[15]School of Geosciences, University of Edinburgh, Edinburgh, UK
[16]Department of Biology, University of Oxford, Oxford, UK
[17]Department of Geographical Sciences, University of Maryland, College Park, Maryland, USA
[18]School of Informatics, Computing, and Cyber Systems, Northern Arizona University Flagstaff, Flagstaff, Arizona, USA
[19]Department of Geography, University College London, London, UK
[20]NERC National Centre for Earth Observation, Leicester, UK

ACKNOWLEDGMENTS

We thank the numerous field workesrs who contributed the TLS and forest inventory datasets used in this study, as well as the institutions and funding agencies involved in these projects. Data collection in Paracou (French Guiana) was carried out as part of the Forestscan (contract AO/1-9584/18/NL/AI) and QA4EO (contract AO/1-9629/19/I-NS) contracts funded by ESA-ESRIN. Paracou research station is managed by CIRAD-UMR EcoFoG (https://paracou.cirad.fr) and benefitted from funding from the Investissement d'Avenir grants of the ANR, France (CEBA: ANR-10-LABX-0025). We thank Mike Liddell, Matt Bradford for access to TERN infrastructure at Robson Creek. TERN (http://www.tern.org.au) is supported by the Australian Government through the National Collaborative Infrastructure. TLS fieldwork in Australia was funded by BELSPO (Belgian Science Policy Office) in the frame of the STEREO III programme - project 3D-FOREST (SR/02/355). L.T. was supported by special research fund (BOF) from Ghent University. TJ was supported by a UK NERC Independent Research Fellowship (grant: NE/S01537X/1). During the preparation of this manuscript, FM was funded by the FWO as a senior postdoc and is thankful to this funding agency for its support (FWO grant n° 1214723 N).

CONFLICT OF INTEREST STATEMENT

The authors declare that there is no conflict of interest.

DATA AVAILABILITY STATEMENT

The data that support the findings of this study are openly available in Tree_Allometry_Discrepancies at https://doi.org/10.5281/zenodo.13149322.

ORCID

Louise Terryn https://orcid.org/0000-0001-8405-2788
Kim Calders https://orcid.org/0000-0002-4562-2538
Félicien Meunier https://orcid.org/0000-0003-2486-309X
Marijn Bauters https://orcid.org/0000-0003-0978-6639
Pascal Boeckx https://orcid.org/0000-0003-3998-0010
Benjamin Brede https://orcid.org/0000-0001-9253-4517
Jerome Chave https://orcid.org/0000-0002-7766-1347
Barbara D'hont https://orcid.org/0000-0002-8136-8899
Mathias Disney https://orcid.org/0000-0002-2407-4026
Tommaso Jucker https://orcid.org/0000-0002-0751-6312
Alvaro Lau https://orcid.org/0000-0002-0419-7002
Susan G. W. Laurance https://orcid.org/0000-0002-2831-2933
Eduardo Eiji Maeda https://orcid.org/0000-0001-7932-1824
Patrick Meir https://orcid.org/0000-0002-2362-0398
Sruthi M. Krishna Moorthy https://orcid.org/0000-0002-6838-2880
Matheus Henrique Nunes https://orcid.org/0000-0001-9979-6456
Alexander Shenkin https://orcid.org/0000-0003-2358-9367
Thomas Sibret https://orcid.org/0000-0002-1496-3444
Tom E. Verhelst https://orcid.org/0000-0003-3138-1558
Phil Wilkes https://orcid.org/0000-0001-6048-536X
Hans Verbeeck https://orcid.org/0000-0003-1490-0168

REFERENCES

Ali, A., & Wang, L.-Q. (2021). Big-sized trees and forest functioning: Current knowledge and future perspectives. *Ecological Indicators*, *127*, 107760.

Anderson-Teixeira, K. J., Davies, S. J., Bennett, A. C., Gonzalez-Akre, E. B., Muller-Landau, H. C., Joseph Wright, S., Abu Salim, K., Almeyda Zambrano, A. M., Alonso, A., Baltzer, J. L., Basset, Y., Bourg, N. A., Broadbent, E. N., Brockelman, W. Y., Bunyavejchewin, S., Burslem, D. F. R. P., Butt, N., Cao, M., … Zimmerman, J. (2015). Ctfs-forest geo: A worldwide network monitoring forests in an era of global change. *Global Change Biology*, *21*, 528–549.

Avitabile, V., Herold, M., Heuvelink, G. B., Lewis, S. L., Phillips, O. L., Asner, G. P., Armston, J., Ashton, P. S., Banin, L., Bayol, N., Berry, N. J., Boeckx, P., de Jong, B. H. J., DeVries, B., Girardin, C. A. J., Kearsley, E., Lindsell, J. A., Lopez-Gonzalez, G., … Willcock, S. (2016). An integrated pan-tropical biomass map using multiple reference datasets. *Global Change Biology*, *22*, 1406–1420.

Banin, L., Feldpausch, T. R., Phillips, O. L., Baker, T. R., Lloyd, J., Affum-Baffoe, K., Arets, E. J. M. M., Berry, N. J., Bradford, M., Brienen, R. J. W., Davies, S., Drescher, M., Higuchi, N., Hilbert, D. W., Hladik, A., Iida, Y., Salim, K. A., Kassim, A. R., … Lewis, S. L. (2012). What controls tropical forest architecture? Testing environmental, structural and floristic drivers. *Global Ecology and Biogeography*, *21*, 1179–1190.

Batista, J., Couto, H., & Marquesini, M. (2001). Performance of height-diameter relationship models: Analysis in three forest types. *Scientia Forestalis*, *60*, 149–163.

Bauman, D., Fortunel, C., Delhaye, G., Malhi, Y., Cernusak, L. A., Bentley, L. P., Rifai, S. W., Aguirre-Gutiérrez, J., Menor, I. O., Phillips, O. L., & McNellis, B. E. (2022). Tropical tree mortality has increased with rising atmospheric water stress. *Nature*, *608*, 528–533.

Bennett, A. C., McDowell, N. G., Allen, C. D., & Anderson-Teixeira, K. J. (2015). Larger trees suffer most during drought in forests worldwide. *Nature Plants*, *1*, 1–5.

Brede, B., Terryn, L., Barbier, N., Bartholomeus, H. M., Bartolo, R., Calders, K., Derroire, G., Moorthy, S. M. K., Lau, A., Levick, S. R., & Raumonen, P. (2022). Non-destructive estimation of individual tree biomass: Allometric models, terrestrial and uav laser scanning. *Remote Sensing of Environment*, *280*, 113180.

Brown, S. (1997). *Estimating biomass and biomass change of tropical forests: A primer* (Vol. *134*). Food & Agriculture Org.

Bürkner, P.-C. (2017). Brms: An r package for bayesian multilevel models using stan. *Journal of Statistical Software*, *80*, 1–28.

Burt, A., Calders, K., Cuni-Sanchez, A., Gómez-Dans, J., Lewis, P., Lewis, S. L., Malhi, Y., Phillips, O. L., & Disney, M. (2020). Assessment of bias in pan-tropical biomass predictions. *Frontiers in Forests and Global Change*, *3*, 12.

Calders, K., Disney, M. I., Armston, J., Burt, A., Brede, B., Origo, N., Muir, J., & Nightingale, J. (2017). Evaluation of the range accuracy and the radiometric calibration of multiple terrestrial laser scanning instruments for data interoperability. *IEEE Transactions on Geoscience and Remote Sensing*, *55*, 2716–2724.

Calders, K., Newnham, G., Burt, A., Murphy, S., Raumonen, P., Herold, M., Culvenor, D., Avitabile, V., Disney, M., Armston, J., & Kaasalainen, M. (2015). Nondestructive estimates of above-ground biomass using terrestrial laser scanning. *Methods in Ecology and Evolution*, *6*, 198–208.

Calders, K., Verbeeck, H., Burt, A., Origo, N., Nightingale, J., Malhi, Y., Wilkes, P., Raumonen, P., Bunce, R. G., & Disney, M. (2022). Laser scanning reveals potential underestimation of biomass carbon in temperate forest. *Ecological Solutions and Evidence*, *3*, e12197.

Chave, J., Réjou-Méchain, M., Búrquez, A., Chidumayo, E., Colgan, M. S., Delitti, W. B., Duque, A., Eid, T., Fearnside, P. M., Goodman, R. C., & Vieilledent, G. (2014). Improved allometric models to estimate the aboveground biomass of tropical trees. *Global Change Biology*, *20*, 3177–3190.

Condit, R., Lao, S., Singh, A., Esufali, S., & Dolins, S. (2014). Data and database standards for permanent forest plots in a global network. *Forest Ecology and Management*, *316*, 21–31.

Cushman, K., Muller-Landau, H. C., Condit, R. S., & Hubbell, S. P. (2014). Improving estimates of biomass change in buttressed trees using tree taper models. *Methods in Ecology and Evolution*, *5*, 573–582.

Cysneiros, V. C., de Souza, F. C., Gaui, T. D., Pelissari, A. L., Orso, G. A., do Amaral Machado, S., de Carvalho, D. C., & Silveira-Filho, T. B. (2021). Integrating climate, soil and stand structure into allometric models: An approach of site-effects on tree allometry in Atlantic forest. *Ecological Indicators*, *127*, 107794.

Dias, A. S., Dos Santos, K., Dos Santos, F. A. M., & Martins, F. R. (2017). How liana loads alter tree allometry in tropical forests. *Plant Ecology*, *218*, 119–125.

Fayolle, A., Panzou, G. J. L., Drouet, T., Swaine, M. D., Bauwens, S., Vleminckx, J., Biwole, A., Lejeune, P., & Doucet, J.-L. (2016). Taller trees, denser stands and greater biomass in semi-deciduous than in evergreen lowland central African forests. *Forest Ecology and Management*, *374*, 42–50.

Feldpausch, T. R., Banin, L., Phillips, O. L., Baker, T. R., Lewis, S. L., Quesada, C. A., Affum-Baffoe, K., Arets, E. J., Berry, N. J., Bird, M., & Brondizio, E. S. (2011). Height-diameter allometry of tropical forest trees. *Biogeosciences*, *8*, 1081–1106.

Feldpausch, T. R., Lloyd, J., Lewis, S. L., Brienen, R. J., Gloor, M., & Monteagudo Mendoza, A. (2012). Tree height integrated into pantropical forest biomass estimates. *Biogeosciences*, *9*, 3381–3403.

Ferraz, A., Saatchi, S., Mallet, C., & Meyer, V. (2016). Lidar detection of individual tree size in tropical forests. *Remote Sensing of Environment*, *183*, 318–333.

Fick, S. E., & Hijmans, R. J. (2017). Worldclim 2: New 1-km spatial resolution climate surfaces for global land areas. *International Journal of Climatology*, *37*, 4302–4315.

Funk, C., Peterson, P., Landsfeld, M., Pedreros, D., Verdin, J., Shukla, S., Husak, G., Rowland, J., Harrison, L., Hoell, A., & Michaelsen, J. (2015). The climate hazards infrared precipitation with stations—A new environmental record for monitoring extremes. *Scientific Data*, *2*, 1–21.

Gatti, L. V., Basso, L. S., Miller, J. B., Gloor, M., Gatti Domingues, L., Cassol, H. L., Tejada, G., Aragão, L. E., Nobre, C., Peters, W., & Marani, L. (2021). Amazonia as a carbon source linked to deforestation and climate change. *Nature*, *595*, 388–393.

Gonzalez de Tanago, J., Lau, A., Bartholomeus, H., Herold, M., Avitabile, V., Raumonen, P., Martius, C., Goodman, R. C., Disney, M., Manuri, S., & Burt, A. (2018). Estimation of above-ground biomass of large tropical trees with terrestrial lidar. *Methods in Ecology and Evolution*, *9*, 223–234.

Harris, D. J., Ndolo Ebika, S. T., Sanz, C. M., Madingou, M. P., & Morgan, D. B. (2021). Large trees in tropical rain forests require big plots. *Plants, People, Planet*, *3*, 282–294.

Hopkinson, C., Chasmer, L., Young-Pow, C., & Treitz, P. (2004). Assessing forest metrics with a ground-based scanning lidar. *Canadian Journal of Forest Research*, *34*, 573–583.

Hubau, W., Lewis, S. L., Phillips, O. L., Affum-Baffoe, K., Beeckman, H., Cun-Sanchez, A., Daniels, A. K., Ewango, C. E., Fauset, S., Mukinzi, J. M., & Sheil, D. (2020). Asynchronous carbon sink saturation in African and Amazonian tropical forests. *Nature*, *579*, 80–87.

Hunter, M., Keller, M., Victoria, D., & Morton, D. C. (2013). Tree height and tropical forest biomass estimation. *Biogeosciences*, *10*, 8385–8399.

Imani, G., Boyemba, F., Lewis, S., Nabahungu, N. L., Calders, K., Zapfack, L., Riera, B., Balegamire, C., & Cuni-Sanchez, A. (2017). Height-diameter allometry and above ground biomass in tropical montane forests: Insights from the albertine rift in Africa. *PLoS One*, *12*, e0179653.

IPCC. (2022). Contribution of working group ii to the sixth assessment report of the intergovernmental panel on climate change.

Jucker, T., Caspersen, J., Chave, J., Antin, C., Barbier, N., Bongers, F., Dalponte, M., van Ewijk, K. Y., Forrester, D. I., Haeni, M., & Higgins, S. I. (2017). Allometric equations for integrating remote sensing imagery into forest monitoring programmes. *Global Change Biology*, *23*, 177–190.

Jucker, T., Fischer, F. J., Chave, J., Coomes, D. A., Caspersen, J., Ali, A., Loubota Panzou, G. J., Feldpausch, T. R., Falster, D., Usoltsev, V. A., & Adu-Bredu, S. (2022). Tallo: A global tree allometry and crown architecture database. *Global Change Biology*, *28*, 5254–5268.

Kearsley, E., De Haulleville, T., Hufkens, K., Kidimbu, A., Toirambe, B., Baert, G., Huygens, D., Kebede, Y., Defourny, P., Bogaert, J., & Beeckman, H. (2013). Conventional tree height–diameter relationships significantly overestimate aboveground carbon stocks in the central Congo basin. *Nature Communications*, *4*, 2269.

Kunz, M., Barrios, H., Dan, M., Dogirama, I., Gennaretti, F., Guillemette, M., Koller, A., Madsen, C., Lana, G., Ortega, A., Ortega, M., Paripari, J., Piperno, D., Reich, K. F., Simon, T., Solis, F., Solis, P., Valdes, J., … Potvin, C. (2022). Bacurú drõa: Indigenous forest custody as an effective climate change mitigation option. A case study from Darién, Panama. *Frontiers in Climate*, *4*, 1047832.

Lapola, D. M., Pinho, P., Barlow, J., Aragão, L. E., Berenguer, E., Carmenta, R., Liddy, H. M., Seixas, H., Silva, C. V., Silva-Junior, C. H., & Alencar, A. A. (2023). The drivers and impacts of amazon forest degradation. *Science*, *379*, eabp8622.

Larjavaara, M., & Muller-Landau, H. C. (2013). Measuring tree height: A quantitative comparison of two common field methods in a moist tropical forest. *Methods in Ecology and Evolution*, *4*, 793–801.

Lau, A., Calders, K., Bartholomeus, H., Martius, C., Raumonen, P., Herold, M., Vicari, M., Sukhdeo, H., Singh, J., & Goodman, R. C. (2019). Tree biomass equations from terrestrial lidar: A case study in Guyana. *Forests*, *10*, 527.

Laurin, G. V., Ding, J., Disney, M., Bartholomeus, H., Herold, M., Papale, D., & Valentini, R. (2019). Tree height in tropical forest as measured by different ground, proximal, and remote sensing instruments, and impacts on above ground biomass estimates. *International Journal of Applied Earth Observation and Geoinformation*, *82*, 101899.

Luo, Y., & Al-Harbi, K. (2017). Performances of loo and waic as irt model selection methods. *Psychological Test and Assessment Modeling*, *59*, 183.

Martnez Cano, I., Muller-Landau, H. C., Wright, S. J., Bohlman, S. A., & Pacala, S. W. (2019). Tropical tree height and crown allometries for the barro colorado nature monument, Panama: A comparison of alternative hierarchical models incorporating interspecific variation in relation to life history traits. *Biogeosciences*, *16*, 847–862.

Morley, S. K., Brito, T. V., & Welling, D. T. (2018). Measures of model performance based on the log accuracy ratio. *Space Weather*, *16*, 69–88.

Ojoatre, S., Zhang, C., Hussin, Y. A., Kloosterman, H. E., & Ismail, M. H. (2019). Assessing the uncertainty of tree height and aboveground biomass from terrestrial laser scanner and hypsometer using airborne lidar data in tropical rainforests. *IEEE Journal of Selected Topics in Applied Earth Observations and Remote Sensing*, *12*, 4149–4159.

Puliti, S., Pearse, G., Surovỳ, P., Wallace, L., Hollaus, M., Wielgosz, M., & Astrup, R. (2023). For-instance: A uav laser scanning benchmark dataset for semantic and instance segmentation of individual trees. *arXiv*. https://doi.org/10.48550/arXiv.2309.01279

Santoro, M., Cartus, O., Carvalhais, N., Rozendaal, D., Avitabilie, V., Araza, A., De Bruin, S., Herold, M., Quegan, S., Rodríguez-Veiga, P., & Balzter, H. (2020). The global forest above-ground biomass pool for 2010 estimated from high-resolution satellite observations. *Earth System Science Data Discussions*, *2020*, 1–38.

Schneider, F. D., Kükenbrink, D., Schaepman, M. E., Schimel, D. S., & Morsdorf, F. (2019). Quantifying 3d structure and occlusion in dense tropical and temperate forests using close-range lidar. *Agricultural and Forest Meteorology*, *268*, 249–257.

Seidel, D., Fleck, S., & Leuschner, C. (2012). Analyzing forest canopies with ground-based laser scanning: A comparison with hemispherical photography. *Agricultural and Forest Meteorology*, *154*, 1–8.

Silva Junior, C. H., Anderson, L. O., Silva, A. L., Almeida, C. T., Dalagnol, R., Pletsch, M. A., Penha, T. V., Paloschi, R. A., & Aragão, L. E. (2019). Fire responses to the 2010 and 2015/2016 Amazonian droughts. *Frontiers in Earth Science*, *7*, 97.

Silva Junior, C. H. L., Campanharo, W. A., Anderson, L. O., & Aragão, L. E. O. C. (2021). Global CHIRPS MCWD (maximum cumulative water deficit) dataset.

Sivula, T., Magnusson, M., Matamoros, A. A., & Vehtari, A. (2020). Uncertainty in bayesian leave-one-out cross-validation based model comparison. *arXiv*. https://doi.org/10.48550/arXiv.2008.10296

Sullivan, M. J., Lewis, S. L., Hubau, W., Qie, L., Baker, T. R., Banin, L. F., Chave, J., Cuni-Sanchez, A., Feldpausch, T. R., Lopez-Gonzalez, G., & Arets, E. (2018). Field methods for sampling tree height for tropical forest biomass estimation. *Methods in Ecology and Evolution*, *9*, 1179–1189.

Tansey, K., Selmes, N., Anstee, A., Tate, N., & Denniss, A. (2009). Estimating tree and stand variables in a corsican pine woodland from terrestrial laser scanner data. *International Journal of Remote Sensing*, *30*, 5195–5209.

Tavares, J. V., Oliveira, R. S., Mencuccini, M., Signori-Müller, C., Pereira, L., Diniz, F. C., Gilpin, M., Marca Zevallos, M. J., Salas Yupayccana, C. A., Acosta, M., & Pérez Mullisaca, F. M. (2023). Basin-wide variation in tree hydraulic safety margins predicts the carbon balance of Amazon forests. *Nature*, *617*, 1–7.

Terryn, L., Calders, K., Åkerblom, M., Bartholomeus, H., Disney, M., Levick, S., Origo, N., Raumonen, P., & Verbeeck, H. (2023). Analysing individual 3D tree structure using the r package ITSMe. *Methods in Ecology and Evolution*, *14*, 231–241.

Terryn, L., Calders, K., Bartholomeus, H., Bartolo, R. E., Brede, B., D'hont, B., Disney, M., Herold, M., Lau, A., Shenkin, A., Whiteside, T. G., & Verbeeck, H. (2022). Quantifying tropical forest structure through terrestrial and uav laser scanning fusion in australian rainforests. *Remote Sensing of Environment*, *271*, 112912.

Tofallis, C. (2015). A better measure of relative prediction accuracy for model selection and model estimation. *Journal of the Operational Research Society*, *66*, 1352–1362.

Wilkes, P., Disney, M. I., Armston, J., Bartholomeus, H., Bentley, L. P., Brede, B., Burt, A., Calders, K., Chavana-Bryant, C., Clewley, D., & Duncanson, L. (2022). Tls2trees: A scalable tree segmentation pipeline for tls data. *bioRxiv*. https://doi.org/10.1111/2041-210X.14233

Wilkes, P., Lau, A., Disney, M., Calders, K., Burt, A., de Tanago, J. G., Bartholomeus, H., Brede, B., & Herold, M. (2017). Data acquisition considerations for terrestrial laser scanning of forest plots. *Remote Sensing of Environment*, *196*, 140–153.

Zhou, X., Yang, M., Liu, Z., Li, P., Xie, B., & Peng, C. (2021). Dynamic allometric scaling of tree biomass and size. *Nature Plants*, *7*, 42–49.

SUPPORTING INFORMATION

Additional supporting information can be found online in the Supporting Information section at the end of this article.

How to cite this article: Terryn, L., Calders, K., Meunier, F., Bauters, M., Boeckx, P., Brede, B., Burt, A., Chave, J., da Costa, A. C. L., D'hont, B., Disney, M., Jucker, T., Lau, A., Laurance, S. G. W., Maeda, E. E., Meir, P., Krishna Moorthy, S. M., Nunes, M. H., Shenkin, A., … Verbeeck, H. (2024). New tree height allometries derived from terrestrial laser scanning reveal substantial discrepancies with forest inventory methods in tropical rainforests. *Global Change Biology*, *30*, e17473. https://doi.org/10.1111/gcb.17473